Design of Broadband and Ultra-Narrowband Tunable Metasurface Absorber Based on Hybrid Ceramic and Vanadium Dioxide Materials

KE JIANG[1], and XUFENG JING[2,*]

[1]*Institute of Optoelectronic Technology, China Jiliang University, Hangzhou, 310018, People's Republic of China*
[2]*College of Information Engineering, China Jiliang University, Hangzhou 310018, PR China*
**Corresponding Author: jingxufeng@cjlu.edu.cn;*

Submission: 2026-07-05; Acceptance: 2026-07-20; Publication: 2027-07-31

With the rapid advancement of terahertz (THz) technology, metasurface absorbers featuring high-efficiency absorption and dynamic tunability have exhibited broad application prospects in fields such as stealth technology, sensing, and energy regulation. However, conventional metallic absorbers suffer from inherent issues including high loss and insufficient tunability. To address these drawbacks, this paper proposes and designs a tunable terahertz metasurface absorber based on an alumina dielectric structure integrated with an ultra-thin vanadium dioxide (VO_2) coating.

The structure utilizes the Mie resonance of alumina dielectric units to localize electromagnetic energy, and achieves dynamic modulation of absorption performance through the drastic conductivity variation induced by the phase transition of VO_2. Simulation results demonstrate that when VO_2 is in its metallic state, the absorber exhibits exceptional broadband absorption characteristics within the 0.3–1.0 THz frequency range, with a relative bandwidth of 107.7% and a peak absorption rate reaching 99.3%. In contrast, when VO_2 transitions to its insulating state, the absorber realizes ultra-narrowband absorption at approximately 0.88 THz with a
bandwidth of merely 0.005 THz and an absorption rate exceeding 98.5%. Moreover, the absorber maintains favorable stability under diverse polarizations and incident angles, exhibiting an extremely high modulation depth and switching ratio.

Further analysis of electromagnetic fields and impedance reveals the underlying physical mechanisms: broadband absorption originates from the synergistic effect of dielectric resonance and ohmic loss in VO_2, whereas ultra-narrowband absorption is dominated by the Fabry-Pérot resonance effect. This research provides a novel design strategy for developing low-loss, dynamically tunable, and structurally stable terahertz wave-absorbing devices, holding significant application value in terahertz stealth technology, intelligent sensing, reconfigurable communications, and other related fields.

Keywords: Terahertz band; Alumina ceramic; Vanadium dioxide; Phase transition modulation; Absorber

1.Introduction

In recent years, metamaterials, as emerging artificial electromagnetic materials [1-3], have enabled flexible manipulation of permittivity and permeability by designing periodically arranged structural units at the subwavelength scale, providing a novel approach for high-efficiency electromagnetic wave absorption technology. Conventional metamaterial absorbers are mostly constructed based on metallic microstructures (e.g., LC resonators). However, such structures face significant challenges in the terahertz (THz) band: high ohmic loss, low quality factor, and absorption performance susceptible to the polarization and incident angle of electromagnetic waves [4-9]. Furthermore, metallic materials tend to excite surface plasmons at high frequencies, causing unnecessary energy dissipation and thus limiting device efficiency and long-term stability. Therefore, the development of all-dielectric absorbing structures with low loss, high stability and dynamic tunability has become an important trend in the research of terahertz functional devices. As a typical dielectric material with high permittivity and low loss, alumina ceramic exhibits excellent dielectric properties ($\varepsilon \approx 9.8$, $\tan\delta < 0.005$) and favorable thermal stability in the terahertz band, making it an ideal candidate for constructing all-dielectric metasurfaces [10]. The utilization of alumina to build Mie resonance units can effectively enhance the localization intensity of electromagnetic fields, suppress radiation loss, and thereby achieve high-efficiency terahertz wave absorption. Nevertheless, traditional dielectric absorbing structures usually possess fixed permittivity, which makes it difficult to dynamically regulate absorption performance and restricts their applications in reconfigurable devices. To realize active modulation of terahertz wave absorption, researchers have introduced various phase-change materials in recent years. Among them, vanadium dioxide (VO_2) has attracted extensive attention due to its unique insulator-to-metal transition (IMT) characteristic. VO_2 undergoes a reversible crystal structure transition at approximately 68 °C, during which its conductivity increases by 4–5 orders of magnitude, accompanied by drastic changes in permittivity and optical constants, thus

exhibiting strong electromagnetic modulation capability in the terahertz band [11-12]. Metasurface structures based on VO_2 can realize real-time switching of absorptivity, reflectivity and even operating frequency points via external excitation, providing a key material basis for tunable terahertz absorbers.

Against this background, this paper proposes a tunable terahertz metasurface absorber combining an all-dielectric alumina structure with an ultra-thin VO_2 coating. This structure uses alumina dielectric units to excite multi-order Mie resonances, realizing effective capture and energy localization of incident terahertz waves. Furthermore, by tuning the conductivity of VO_2 through its insulator-to-metal phase transition, the dissipation process of electromagnetic energy is controlled, enabling dynamic switching between broadband absorption and ultra-narrowband absorption modes.

In this paper, the absorption characteristics, field distribution and modulation mechanism of the absorber under different phase states are systematically analyzed via full-wave electromagnetic simulation. The results show that when VO_2 is in the metallic state, the structure achieves an absorptivity exceeding 80% in the 0.3–1.0 THz band with a peak absorptivity of 99.3%, demonstrating excellent broadband absorption performance. When VO_2 is in the insulating state, the absorber presents ultra-narrowband absorption at approximately 0.88 THz with a bandwidth of only 0.005 THz and an absorptivity up to 98.5%, featuring remarkable switching characteristics and modulation depth. In addition, the structure exhibits favorable stability under different polarizations and incident angles, possessing good practical potential. This research provides a new design strategy for developing low-loss, tunable and high-stability terahertz absorbing devices, with significant application prospects in terahertz stealth, communication modulation, energy harvesting and other fields.

2.Structural Design of the Absorber

In this paper, a terahertz metasurface absorber is designed based on the coupling between an all-dielectric alumina microstructure and an ultra-thin vanadium dioxide (VO_2) functional film. The three-dimensional unit cell structure is illustrated in Fig. 1(a). The entire structure is constructed from an integrated alumina substrate, with a uniform VO_2 film of only 0.1 μm thickness coated on both the top and bottom surfaces of the unit cell. Alumina exhibits a high relative permittivity and extremely low dielectric loss in the terahertz band, making it an ideal dielectric material for stably supporting electromagnetic Mie resonance modes. Consequently, its geometric dimensions directly determine the resonant frequencies, mode types, and spatial distribution of the localized electromagnetic fields of the absorber.

The alumina substrate is fabricated via precision micromachining to form a three-dimensional dielectric microstructure with a specific electromagnetic response. As shown in Fig. 1(b), its top surface consists of four equally spaced and regularly arranged elliptical cylinders, together with a central cylindrical dielectric protrusion. This five-element composite scattering structure not only maintains strict central symmetry in the plane but also can simultaneously excite multi-order Mie electromagnetic resonances in the terahertz band. Through the near-field electromagnetic coupling between adjacent resonators, more complex hybrid modes are formed, thereby achieving absorption bandwidth broadening and absorption efficiency enhancement.

The unit cell period is set to p = 400 μm, the thickness of the alumina base is h_1 = 400 μm, and the height of the four elliptical protrusions and the central cylindrical protrusion is h_2 = 100 μm. The minor and major axes of the ellipses are a = 80 μm and b = 160 μm, respectively, and the diameter of the central circle is R = 120 μm.

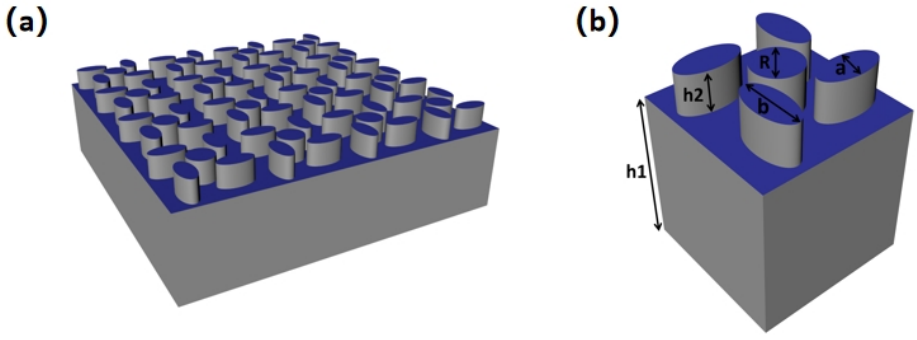

Figure 2.1 Schematic diagram of the metamaterial absorber: (a) Schematic of the array structure; (b) Schematic of the unit cell structure.

3.Working Principle and Performance of the Absorber

Alumina ceramic features a high relative permittivity ($\varepsilon \approx 9.8$) and an extremely low loss tangent ($\tan\delta < 0.005$), enabling robust support for Mie resonances in the terahertz

band. In the proposed design, the geometric configuration of alumina excites multiple electromagnetic resonance modes, including the electric dipole (ED) mode and magnetic dipole (MD) mode. These resonances lay the fundamental basis for high-efficiency absorption of the absorber. Owing to its high permittivity and low loss, alumina effectively reinforces these resonance modes and yields superior absorption performance in the terahertz regime. Furthermore, the low-loss characteristic of alumina preserves a high quality factor (Q-factor) during operation, ensuring stable and strong electromagnetic field localization and absorption under prolonged working conditions. This is critical for designing broadband and high-efficiency absorbers; especially in environments with large temperature variations, the high stability and high thermal conductivity of alumina guarantee reliable device operation. As a ceramic material, alumina also enhances the mechanical stability and reliability of the metasurface. Compared with metallic materials, alumina exhibits stronger oxidation resistance and deformation resistance, particularly at elevated temperatures, which greatly improves reliability in high-power applications and mitigates performance degradation of metals under extreme conditions. From a fabrication perspective, the superior physical properties of alumina offer distinct advantages in high-precision magnetron sputtering, especially during the deposition of vanadium dioxide coatings, making it an ideal substrate for high-accuracy manufacturing.

Vanadium dioxide (VO_2) is a phase-change material with remarkable transition characteristics, whose temperature-driven phase change grants it extensive application potential in optoelectronic and terahertz technologies. VO_2 is insulating at room temperature and undergoes an insulator-to-metal transition (IMT) at approximately 68 °C. This transition is accompanied by a drastic surge in electrical conductivity and pronounced modifications of optical properties, establishing VO_2 as a high-performance tunable phase-change material. The phase transition of VO_2 originates from a crystal structural change: as illustrated in Fig. 3(a), it adopts a monoclinic structure at low temperatures with high electrical resistivity, and transforms into a rutile structure at high temperatures with metallic behavior. As temperature rises, the molecular arrangement rearranges, notably the relative positions of vanadium and oxygen atoms, leading to substantial variations in conductivity and permittivity. Such a reversible insulator-to-metal transition renders VO_2 ideal for tunable optoelectronic devices, enabling dynamic modulation over a wide temperature range.

In its low-temperature insulating state, VO_2 exhibits high terahertz transmittance, whereas transmittance drops sharply upon transition to the metallic state due to intensified plasmonic oscillations. This behavior unlocks strong application potential in the terahertz band. The conductivity of VO_2 changes by four to five orders of magnitude across the phase transition, providing a wide dynamic tuning range and high modulation depth for metamaterial-based optoelectronic devices. The permittivity and conductivity of VO_2 can be described by the Drude model, with its complex permittivity expressed as:

$$\varepsilon(\omega)_{VO_2}=\varepsilon_\infty-\frac{\omega_p^2}{\omega(\omega+i\gamma_2)} \qquad (3\text{-}1)$$

In the Drude model given by Eq. (3-1), the high-frequency permittivity of VO_2 is set as $\varepsilon_\infty = 12$, and $\gamma_2 = 5.75\times10\text{^}13$ rad/s denotes the collision frequency. The electrical conductivity σ of VO_2 changes drastically during the phase transition. The temperature dependence of conductivity under thermal control is plotted in Fig. 3(b). At room temperature, VO_2 is insulating with a conductivity of approximately 20 S/m. As temperature increases and reaches the phase-transition threshold, VO_2 abruptly switches from the insulating state to the metallic state, with conductivity surging to 2×10^5 S/m. This transition is fully reversible: upon cooling, VO_2 reverts to the insulating state. The pronounced conductivity variation of VO_2 with temperature mainly stems from temperature-induced permittivity modulation. Fig. 3(b) and Fig. 3(d) present the evolution of the real part （ε′） and imaginary part （ε″） of the permittivity of VO_2 at different conductivity levels, respectively. It can be seen that （ε′） is consistently much larger than （ε″） across the measured range, indicating a loss-dominated response. Meanwhile, the dielectric response is particularly acute near the phase-transition region corresponding to the steep conductivity change.

Based on the above properties, the phase transition of VO_2 is commonly controlled via the following methods:Thermally induced phase transition: Heating the metallic layer at the bottom of the absorber conducts heat to the VO_2 layer, driving the transition from insulation to metallic conduction with gradually increasing conductivity. After removing the heat source, cooling reverses the transition and reduces conductivity.Joule-heating induced phase transition: Depositing metallic electrodes on the VO_2 layer and applying a voltage across the electrodes generates Joule heat, which transfers to VO_2 and triggers the insulator-to-metal transition. After removing the voltage, cooling restores the insulating state.In addition, chemical doping can also be employed to induce the insulator-to-metal transition of VO_2.

By means of the above phase-transition control strategies, switching the electrical state of VO_2 enables the absorber to toggle between broadband and ultra-narrowband operating modes, offering an effective route for the design and application of multifunctional tunable optoelectronic devices.

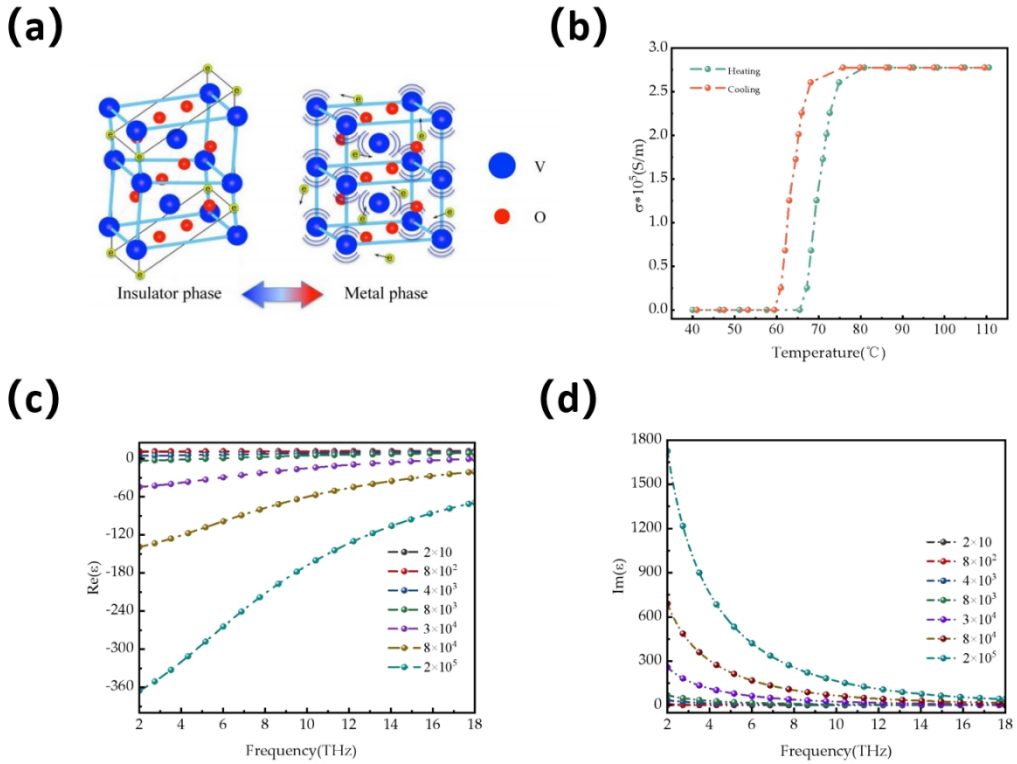

Figure 3.1 Properties of vanadium dioxide: (a) Crystal structure; (b) Variation curve of conductivity with ambient temperature; (c) Real part of permittivity under different conductivities; (d) Imaginary part of permittivity under different conductivities.

In this work, the full-wave electromagnetic simulation method is adopted to systematically investigate the absorption characteristics, field distributions and modulation mechanisms of the phase-change modulated metamaterial absorber based on vanadium dioxide. The simulations are carried out in the time-domain solver of Computer Simulation Technology Microwave Studio (CST) utilizing the Finite Integration Technique (FIT). By extracting the reflectivity R and transmittance T, the absorption spectrum is obtained according to the absorptivity formula \(A=1-R-T\). In the simulation model, periodic boundary conditions are applied along the x and y directions, and perfectly matched layers (PMLs) are employed along the z direction.

The simulated results are presented in Fig. 3.2(a). When VO_2 is in the metallic state, the absorber exhibits outstanding broadband absorption performance. The absorptivity remains above 80% within the 0.3–1.0 THz band, yielding an absolute absorption bandwidth of 0.7 THz and a relative absorption bandwidth of 107.7%. Nearly perfect absorption of 99% is achieved at 0.494 THz. The impedance matching theory is used to analyze the performance of the terahertz metamaterial absorber. For intuitive understanding, the reflectivity R and transmittance T are also plotted in Fig. 3.2(b). When VO_2 serves as the functional layer, the transmittance T is almost negligible. In accordance with the Effective Medium Theory (EMT), the proposed absorber can be equivalent to a homogeneous dielectric layer. As shown in Fig. 3.2(c), the real and imaginary parts of the normalized impedance (Z) of the metamaterial absorber are retrieved via the S-parameter inversion method. At low frequencies, the real and imaginary parts of the normalized impedance deviate greatly from the impedance of free space, leading to low absorption efficiency. As frequency rises, the real part of the normalized impedance gradually approaches unity while the imaginary part tends toward zero. Under such circumstances, characteristic impedance matching between the absorber and free space is realized. Optimal impedance matching occurs at 0.494 THz, corresponding to the maximum absorptivity, which agrees well with theoretical expectation. When VO_2 transitions to the insulating state, the absorber realizes ultra-narrowband absorption ranging from 0.88 THz to 0.885 THz. The full absorption bandwidth is merely 0.005 THz with a peak absorptivity up to 98.5%. Such obvious discrepancy in absorption responses demonstrates the excellent modulation capability and switching performance enabled by the phase transition of VO_2.

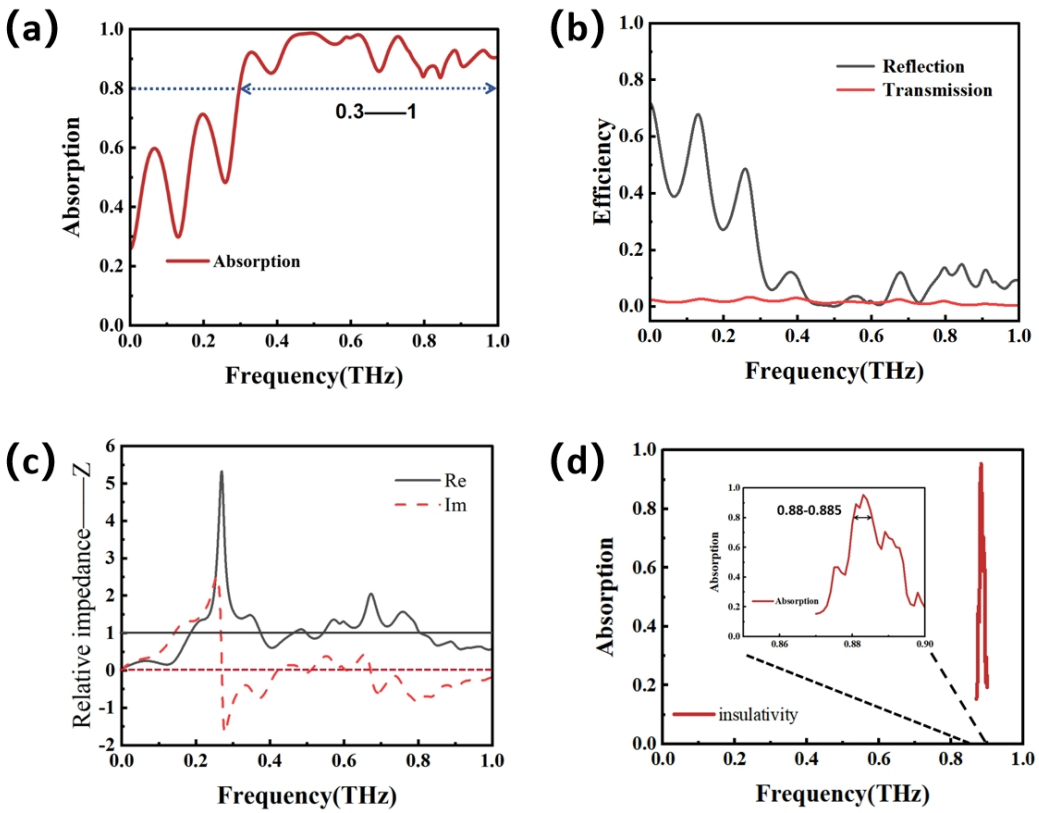

Figure 3.2 Absorber: (a) Broadband absorption spectrum; (b) Reflectivity R and transmittance T; (c) Real and imaginary parts under impedance matching condition; (d) Ultra-narrowband absorption curve at 0.88 THz

4.Full-Wave Electromagnetic Simulation and Analysis of Incident Angle

To gain an in-depth understanding of the physical mechanism of the metamaterial absorber, full-wave electromagnetic simulations are carried out. The resonant modes correspond to waveguide modes, which are hybrid modes composed of magnetic (EH) modes and electric (HE) modes. Specifically, the EH mode is a hybrid mode dominated by the transverse magnetic (TM) mode, while the HE mode is a hybrid mode dominated by the transverse electric (TE) mode. Under these two modes, we evaluate the electric field distribution, magnetic field distribution, current density and energy loss at the resonant frequencies, respectively.

First, a detailed analysis of the absorber under broadband absorption is performed, as illustrated in Figure 4.1(a), and the evaluation is conducted at 0.5 THz. Multiple electromagnetic modes are excited in the absorber at this frequency, among which the strongest resonant modes are the electric dipole (ED) mode and magnetic dipole (MD) mode. At this resonant frequency, the electric field is mainly concentrated on the upper surfaces of the elliptical microstructures and central circles, especially at the edges of vanadium dioxide (VO_2), generating remarkable electric field localization. In contrast, the magnetic field is primarily distributed between the interfaces of the elliptical/central circular microstructures and the underlying substrate, exhibiting obvious magnetic field enhancement. Such localized enhancement of electric and magnetic fields enables the absorber to efficiently capture electromagnetic wave energy and convert it into heat, thus achieving high-efficiency absorption.

Meanwhile, the distributions of electric and magnetic fields reveal that the high permittivity of alumina plays a vital role in electric field localization, strengthening the electric field at the edges of microstructures. Furthermore, the phase transition effect of VO_2 further intensifies the localization of electric and magnetic fields in its metallic state, leading to a notable improvement in the absorption peak.

The wave-absorbing mechanism differs from the broadband absorption when VO_2 is in the insulating state. For one thing, the overall loss of the structure declines owing to the extremely low conductivity of VO_2. Low loss facilitates the maintenance of resonant modes with high quality factors (Q-factors), and a high Q-factor generally corresponds to a sharp absorption peak with narrow bandwidth. For another, Fabry–Pérot (F-P) resonance dominates in this case. F-P resonance occurs in dielectric layers between multiple reflective interfaces; in particular,

light waves undergo multiple reflections and interference at different boundaries. The optical path difference determines the interference conditions at different frequencies, which enhances or suppresses absorption at specific frequencies.

Even with low conductivity of insulating VO_2, F-P resonance can produce constructive interference inside the structure via optical path difference and multiple reflections, resulting in ultra-narrowband absorption. Benefiting from this elaborate design, the metasurface absorber achieves enhanced tunability. As shown in Figure 4(b), the electric field resonant modes are significantly weakened or even eliminated when VO_2 is in the insulating state. This is attributed to the low conductivity of insulating VO_2, which weakens localized electric field enhancement and the concentration of current density, making electric field localization inconspicuous. Consequently, the electric field distribution nearly vanishes at this frequency, and no obvious electromagnetic energy is locally absorbed.

Nevertheless, magnetic induction still exists and concentrates mainly within the alumina dielectric material despite the disappearance of electric field resonance. This indicates that magnetic coupling persists in insulating VO_2, yet the effect is insufficient to support electromagnetic absorption. The corresponding surface current density maps demonstrate that the current density almost disappears when VO_2 is insulating, meaning no current flows along the structural surface.

Further analysis of energy loss shows that energy dissipation still exists inside alumina, especially at the alumina–VO_2 interface. This phenomenon is closely associated with Fabry–Pérot (F-P) resonance. Although insulating VO_2 features low conductivity, F-P resonance remains effective inside the structure. Specifically, electromagnetic waves reflect and interfere between alumina and VO_2, generating constructive interference. Energy is gradually absorbed during multiple reflections within these dielectric layers. Such interference concentrates partial electromagnetic energy inside the alumina dielectric layer and triggers localized energy dissipation, manifested as absorption and loss, and ultimately produces ultra-narrowband absorption within this frequency range.

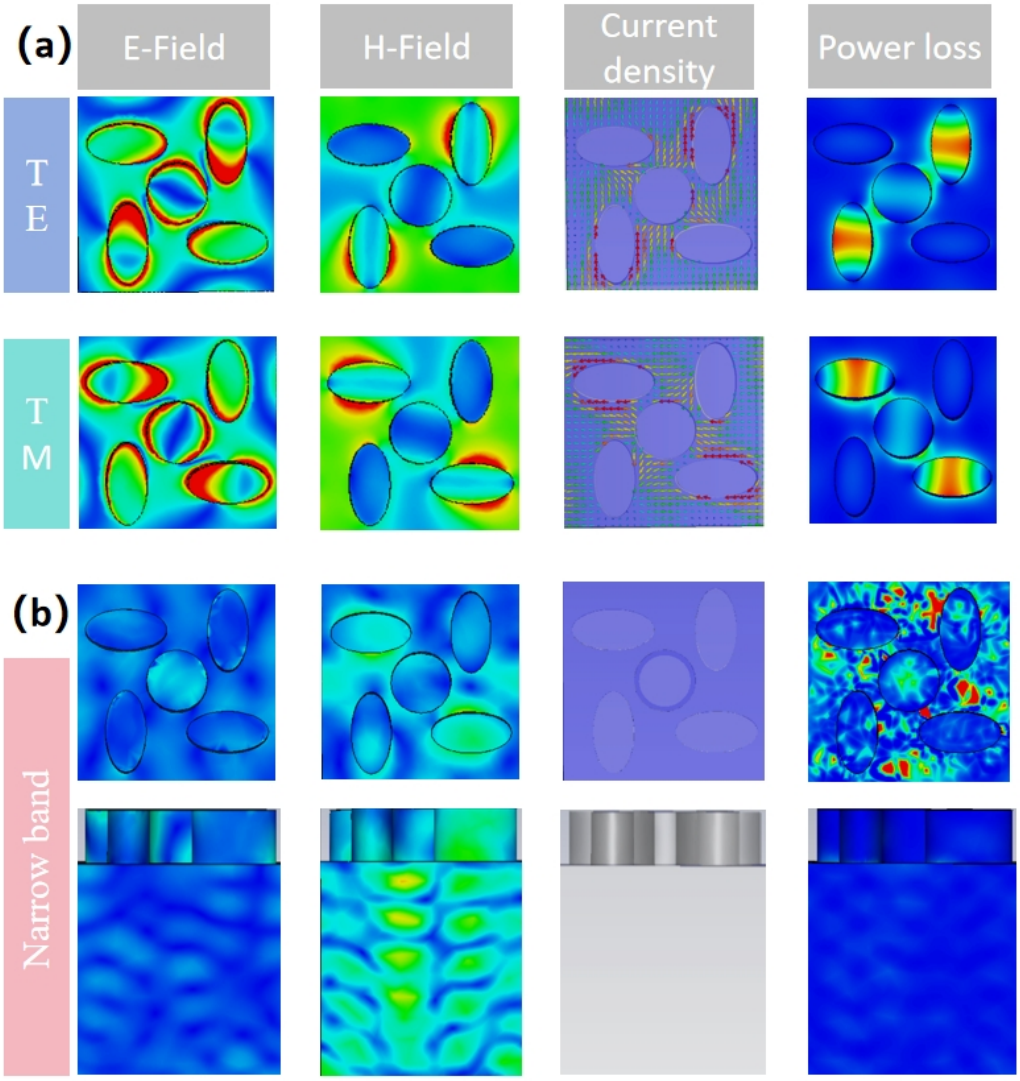

Figure 4.1 Full-wave electromagnetic simulations of the absorber:(a) Distributions of electromagnetic field, current density and energy loss under TE and TM modes for broadband absorption operation; (b) Distributions of electromagnetic field, current density and energy loss of the absorber operating at the ultra-narrowband absorption state.

Subsequently, the absorption characteristics of the metamaterial absorber at different incident angles under transverse electric (TE) and transverse magnetic (TM) polarizations are presented separately. It can be observed that absorption peaks can be achieved for both TE and TM modes under normal incidence. This indicates that the proposed metamaterial absorber can efficiently absorb electromagnetic waves for both modes at normal incidence, achieving near-perfect absorption within the target frequency band. This property originates from the symmetric configuration, rendering the absorber polarization-insensitive.

The influence of incident angle on the performance under the TE mode is illustrated in Figure 4.1(c). As the incident angle \(\theta\) increases from 0° to 75°, the overall performance of the absorber exhibits a declining trend. At a moderate incident angle of 45°, the broadband absorption efficiency remains nearly unchanged; high-efficiency absorption of approximately 80% can still be maintained from 0.3 THz to 1 THz. When the angle exceeds 60°, the absorption curve shifts downward overall, and the broadband absorption performance degrades obviously. This behavior can be readily interpreted: effective electromagnetic resonance weakens with increasing incident angle, accompanied by aggravated impedance mismatch.

By contrast, the angular response under the TM mode differs from that of the TE mode, as shown in Figure 4.1(d). The absorption curves display more drastic and complicated fluctuations compared with the TE mode. In

the low-frequency range (0 THz to 0.3 THz), the absorption performance is even enhanced as the incident angle rises. The broadband absorption region maintains favorable performance at 45°, while obvious attenuation occurs above 60°. Notably, at certain specific frequencies and angles, some frequency bands originally featuring around 80% absorption efficiency can realize near-perfect absorption close to 99%.

Such complex performance arises from the fact that at small and moderate incident angles, oblique incidence modulates the coupling efficiency between surface resonators and incident waves, enabling more energy to be trapped inside the cavity and thus elevating the absorption peaks. At large angles, especially near grazing incidence, the matching condition between the equivalent impedance of the absorber surface for TM waves and the free-space impedance is broken. A larger portion of energy is reflected, leading to reduced absorptivity. Furthermore, the electric field of TM waves contains a component perpendicular to the interface. This component significantly modulates the electromagnetic field distribution and loss mechanism inside dielectric layers, resulting in distinct impedance mismatch behavior for the TM mode at large angles relative to the TE mode. This also explains why the TM mode may achieve better local impedance matching at specific angles and generate near-perfect absorption peaks. Nevertheless, from the perspective of overall broadband absorption, large incident angles remain unfavorable for stable high-performance impedance matching.

For both TE and TM modes, the absorber exhibits relatively robust performance within an incident angle range up to 60° and maintains high absorptivity. It possesses favorable polarization insensitivity and the capability of wide-angle operation.

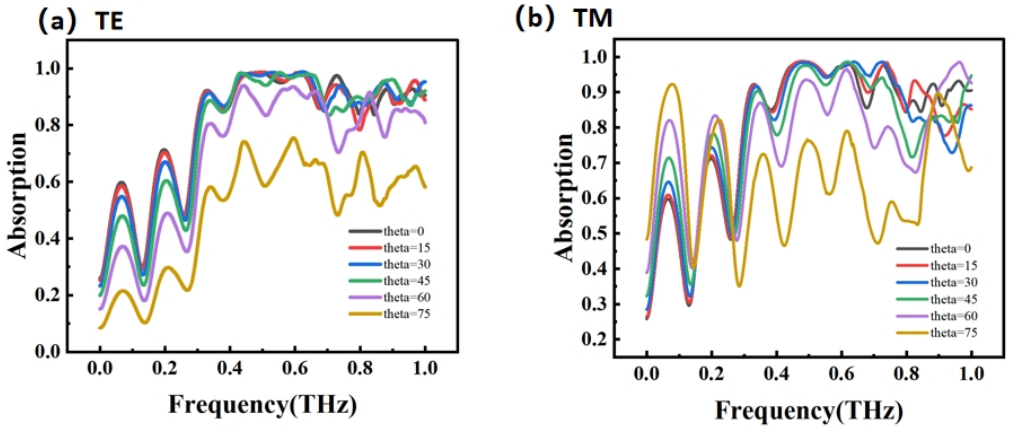

Figure 4.2 Analysis of incident angle: (a) Absorption curves under TE mode; (b) Absorption curves under TM mode

5.Analysis of Structural Parameters

We first investigate the influence of the vanadium dioxide tunable coating on broadband absorption performance. As shown in Figure 5.1(a), variations in the thickness of the vanadium dioxide coating affect the absorption response of the absorber at several specific frequency points (near 0.4 THz and 0.8 THz). When the thickness of vanadium dioxide exceeds 0.2 μm, the absorption efficiency drops below 80%. In contrast, the absorber exhibits excellent ultra-narrowband absorption characteristics at a thickness of 0.1 μm, which provides the necessary structural conditions to excite Fabry–Pérot resonance.

Next, the effect of alumina substrate thickness is analyzed. The dielectric loss properties of alumina have been discussed previously, and its material properties determine that its participation in the absorption process is limited. Figure 5.1(b) further verifies this conclusion. Within the broadband absorption range of 0.3–1 THz, the absorption performance is barely affected by changes in alumina thickness; only a local absorption reduction occurs near 0.3 THz, which is generally consistent with the design expectation. This characteristic offers design freedom for adopting thicker substrates: the thickness of the alumina substrate can be increased when enhanced thermal insulation is required. Meanwhile, the thickness of the vanadium dioxide coating can be adjusted accordingly in the ultra-narrowband absorption design to maintain resonant absorption performance.

As mentioned earlier, broadband absorption originates from complicated hybrid modes formed by electromagnetic near-field coupling between adjacent resonators. To explore the influence of the protrusion on the substrate on overall absorption efficiency, Figure 5.1(c) compares the absorption characteristics of the incomplete structure (without the protruding central circle) and the complete structure (with the protruding central circle) in the frequency range of 0.0–1.0 THz. The complete structure achieves remarkably enhanced absorption at multiple frequency points. Particularly within the 0.3–0.4 THz band, the absorption curve of the complete structure lies consistently above that of the incomplete structure, demonstrating that the introduction of the protruding central circle effectively improves absorption efficiency in this band. In the range of 0.4–0.9 THz, the absorption

curves of the two structures follow similar trends, indicating that the performance in this band is mainly governed by the other four elliptical resonant structures.

Such performance improvement is closely associated with the electromagnetic near-field coupling mechanism described above. The introduction of the protruding central circle modulates the electromagnetic field distribution between adjacent resonators and facilitates the formation of more complex hybrid modes. The coupling between the central circle and surrounding resonant structures strengthens the localization and dissipation of electromagnetic energy on the structural surface, thereby optimizing absorption efficiency in the critical frequency band. It is worth noting that the incomplete structure still maintains high absorptivity near 1 THz, revealing that the resonant structures on the substrate possess favorable inherent wave-absorbing properties. Nevertheless, the complete structure sustains stable high absorption across a wider frequency range, which validates the design philosophy that electromagnetic coupling can be modulated via elaborate structural design to realize optimized broadband performance.

This result further demonstrates that in the design of metamaterial absorbers, not only the arrangement of resonant units matters, but also the fine structural features inside individual resonant units exert a considerable impact on the overall performance. Rational design of secondary structures such as the protruding central circle provides an effective design degree of freedom to tailor the absorption band and optimize absorption efficiency.

To further explore the effects of structural parameters, simulations are carried out by varying the radius of the central circle, and the results are presented in Figure 5.1(d). The figure shows that near 0.4 THz and 0.8 THz, the absorption efficiency increases significantly once the radius of the central circle exceeds 50 μm. This phenomenon again confirms the foregoing viewpoint: outstanding wave-absorbing performance can only be achieved through sophisticated micro-nano structural design.

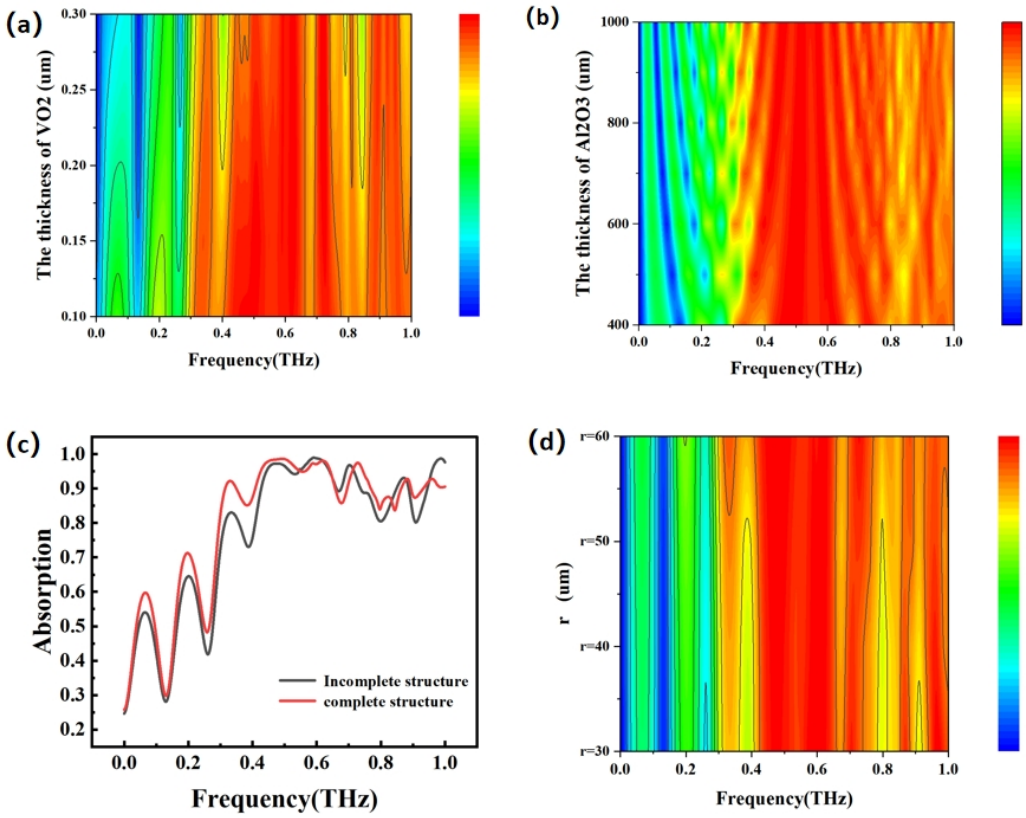

Figure 5.1 Analysis of the effect of structural parameters on absorptivity: (a) Thickness of vanadium dioxide coating; (b) Thickness of alumina ceramic substrate; (c) Structural completeness; (d) Radius r of the central circle

6.Conclusion

In this work, a tunable terahertz metasurface absorber combining an alumina dielectric layer and a vanadium dioxide (VO_2) functional coating is successfully designed and investigated. The proposed design skillfully exploits the high permittivity and low-loss characteristics of alumina as well as the insulator-to-metal phase transition

property of VO_2, enabling dynamic and reversible modulation of terahertz absorption within a single device.

When VO_2 is in the metallic state, the device exhibits broadband absorption with absorptivity exceeding 80% in the frequency range of 0.3–1.0 THz, and the peak absorptivity reaches 99.3%. In the insulating state of VO_2, an ultra-narrowband absorption with a bandwidth as narrow as 0.005 THz emerges near 0.88 THz accompanied by a remarkable modulation depth, demonstrating excellent phase-transition modulation capability.

Electromagnetic simulations and parametric analysis reveal the underlying physical mechanisms. The broadband absorption mainly originates from the synergy between Mie resonance supported by the alumina dielectric structure and ohmic loss of VO_2, whereas the ultra-narrowband absorption is dominated by the Fabry–Pérot resonance effect. Further impedance matching analysis indicates that the structural impedance matches well with free-space impedance at resonant frequencies, which contributes to near-perfect absorption. The angular stability analysis verifies that the absorber possesses favorable polarization insensitivity and wide-angle tolerance within an incident angle of 60°, demonstrating promising practical potential.

From the perspective of structural design, micro-nano features such as the protruding central circle are proven critical for enhancing electromagnetic coupling and optimizing absorption in specific frequency bands. Meanwhile, the thicknesses of the VO_2 coating and alumina substrate offer design freedom for dynamic absorption modulation and structural stability, respectively.

This study provides effective design strategies and theoretical support for developing low-loss, tunable and highly stable terahertz absorbing devices, and holds broad application prospects in terahertz stealth, sensing, communication and other fields. Future work will further explore fast phase-transition schemes such as electrical and optical control, and extend the design toward multifunctional integration and flexible devices.

Reference

[1] A. Nemati, Q. Wang, M. Hong, et al. Opto-Electron. Adv. (2019).

[2] P. Alitalo, S. Tretyakov. Mater. Today 12(3), 22-29 (2009).

[3] U. Leonhardt, T. Tyc. Science 323(5910), 110-112 (2009).

[4] S. Zhao, H. Ma, T. Shao, et al. J. Alloys Compd. 874, 159822 (2021).

[5] B. Zohuri. Radar Energy. 147-203 (2020).

[6] M. Manjappa, P. Pitchappa, N. Wang, et al. Adv. Opt. Mater. 6(16), 1800141 (2018).

[7] B. Wang, W. Yerazunis, K. H. Teo. Proc. IEEE 101(6), 1359-1368 (2013).

[8] A. Alkhateeb, R. W. Heath. IEEE Trans. Commun. 64(5), 1801-1818 (2016).

[9] X. J. He, Y. Wang, J. Wang, et al. Prog. Electromagn. Res. 115, 381-397 (2011).

[10] Z. Wu, Q. Wang, L. Zhang, et al. J. Aeronaut. Mater. 40(1), 9 (2020).

[11] R. Kowerdziej, J. Parka, J. Krupka. Liq. Cryst. 38(6), 743-747 (2011).

[12] Y. Pang, J. Wang, Q. Cheng, et al. Appl. Phys. Lett. 110(10), 104103 (2017).